HU Binding to DNA: Evidence for Multiple Complex Formation and DNA Bending†

Kristi Wojtuszewski,‡ Mary E. Hawkins,§ James L. Cole,|| and Ishita Mukerji*,‡

Molecular Biology and Biochemistry Department, Molecular Biophysics Program, Wesleyan University, Middletown, Connecticut 06459-0175, Pediatric Branch, National Cancer Institute, Building 10/13N240, 10 Center Drive, MSC 1928, Bethesda, Maryland 20892-1928, and WP 44-B122, Department of Antiviral Research, Merck Research Laboratories, West Point, Pennsylvania 19486

Received October 13, 2000; Revised Manuscript Received December 26, 2000

ABSTRACT: HU, a nonspecific histone-like DNA binding protein, participates in a number of genomic events as an accessory protein and forms multiple complexes with DNA. The HU−DNA binding interaction was characterized by fluorescence, generated with the guanosine analogue 3-methyl-8-(2-deoxy-β-D-ribofuranosyl)isoxanthopterin (3-MI) directly incorporated into DNA duplexes. The stoichiometry and equilibrium binding constants of complexes formed between HU and 13 and 34 bp DNA duplexes were determined using fluorescence anisotropy and analytical ultracentrifugation. These measurements reveal that three HU molecules bind to the 34 bp duplexes, while two HU molecules bind to the 13 bp duplex. The data are well described by an independent binding site model, and the association constants for the first binding event for both duplexes are similar ($\sim 1 \times 10^6$ M^{-1}), indicating that HU binding affinity is independent of duplex length. Further analysis of the binding curves in terms of a nonspecific binding model is indicative that HU binding to DNA exhibits little to no cooperativity. The fluorescence intensity also increases upon HU binding, consistent with decreased base stacking and increased solvent exposure of the 3-MI fluorescence probe. These results are suggestive of a local bending or unwinding of the DNA. On the basis of these results we propose a model in which bending of DNA accompanies HU binding. Up to five complex bands are observed in gel mobility shift assays of HU binding to the 34 bp duplexes. We suggest that protein-induced bending of the DNA leads to the observation of complexes in the gel, which have the same molecular weight but different relative mobilities.

HU, a nonspecific histone-like DNA binding protein, is implicated as an accessory protein in a number of genomic events in *Escherichia coli*, including replication, transcription, recombination, and packaging of DNA (*1*). Functioning primarily as an architectural protein similar to HMG, HU facilitates the binding of other proteins to their target sequences by either stabilizing DNA in a bent conformation or possibly inducing a bend upon binding (*2*).

The three-dimensional structure of the homodimeric form of *Bacillus stearothermophilus* HU has been solved using X-ray crystallography and NMR methodologies (*3*−*6*). The HU used in this study was isolated from *E. coli* and exists as a stable heterodimer. The two subunits form a relatively compact α-helical core from which two β-sheet arms extend. In integration host factor protein (IHF),[1] which is identical to HU in terms of secondary structure and 40% identical in primary structure, these two β-arms line the minor groove of the DNA as shown by the X-ray cocrystal structure (*7*). In HU these arms are highly flexible, and a similar mechanism of interaction is proposed (*5*−*7*). IHF, in contrast to HU, recognizes a specific DNA sequence and bends the DNA by ∼160° upon binding (*8*).

Nuclease digestion studies have suggested that HU binding alters the helical pitch (*9*), and circularization assays are indicative of DNA bending upon HU binding (*10*, *11*). In previous studies of HU binding to linear DNA, multiple complexes were detected in gel mobility shift assays (GMSA) (*12*), which were indicative of a 9 bp binding site. Recently, footprinting experiments of HU bound to the Mu transpososome (*13*, *14*) or cruciform (*15*, *16*), nicked (*17*, *18*), or supercoiled DNA (*19*) have suggested that HU forms a complex that is structurally similar to the one formed by IHF. Thus, HU promotes specific genomic events, yet binds to DNA independent of base sequence, which argues for a complex mechanism of DNA recognition that is based upon DNA structure and flexibility. This specific binding to DNA appears to be of functional importance and regulated by DNA

† This work was supported by a National Science Foundation Career Development Award (MCB-9507241) and a grant from the Patrick and Catherine Weldon Donaghue Medical Research Foundation (DF96-175). K.W. acknowledges support from an NIH Training Grant in Molecular Biophysics (IT32-GM08271).

* To whom correspondence should be addressed. Phone: 860-685-2422. Fax: 860-685-2141. E-mail: Imukerji@wesleyan.edu.

‡ Wesleyan University.

§ National Cancer Institute.

|| Merck Research Laboratories.

[1] Abbreviations: 3-MI, 3-methyl-8-(2-deoxy-β-D-ribofuranosyl)-isoxanthopterin; GMSA, gel mobility shift assay; bp, base pair; IHF, integration host factor; Int, integrase; DTT, dithiothreitol; EDTA, *N*,*N*,*N*′,*N*′-ethylenediaminetetraacetic acid; HEPES, *N*-(2-hydroxyethyl)-piperazine-*N*′-2-ethanesulfonic acid; Tris, tris(hydroxymethyl)amino-methane.

10.1021/bi002382r CCC: $20.00
Published on Web 02/01/2001

Table 1: Sequence of Oligonucleotides Used

Oligonucleotide	No. of base pairs	Sequence (**F** = 3-MI)	Position of 3-MI (from 5' end)
H1-34-1[a]	34	5'-tat gca gtc act atg aat caa cta ctt a**F**a tgg t-3' 3'-ata cgt cag tga tac tta gtt gat gaa tct acc a-5'	29
H1-34-2[a]	34	5'-tat gca gtc act atg aat caa cta ctt aga tgg t-3' 3'-ata cgt cag tga tac tta gtt **F**at gaa tct acc a-5'	13
H1-13-1[b]	13	5'- at caa cta cct ta -3' 3'- ta gtt gat g**F**a at -5'	4

[a] In the H1-34-CT oligonucleotide F = g. [b] In the H1-13-CT oligonucleotide F = g.

structure and other accessory factors. These studies address this mechanism of recognition by studying the conformational changes induced in linear DNA upon HU binding using solution methods.

In this study fluorescence anisotropy and analytical ultracentrifugation measurements are used to determine the stoichiometry and equilibrium binding constants of HU binding to 13 and 34 bp duplexes of DNA. The sequences used are based upon the H1 binding site of IHF (Table 1), to which HU binds with high affinity in the presence of the recombinase protein integrase (Int) (*20*). Fluorescence anisotropy directly measures DNA−protein complex formation by the decreased rotational diffusion of the complex and can detect the presence of additional complexes not observable by other methods (*21*−*23*). In addition, specific incorporation of the fluorescent probe into the DNA sequence yields anisotropy values that are more directly reflective of global DNA motion. Analytical ultracentrifugation characterizes the native state of a complex under biologically relevant conditions and was used to determine the assembly of HU−DNA complexes and measure the equilibrium binding constants (*24*, *25*). One strength of both techniques is the ability to measure the weak interactions that typify nonspecific protein−DNA complexes. Analysis of these nonspecific interactions in solution is preferred over more conventional electrophoresis or gel mobility shift assays because there are no contributing influences from the gel matrix, which can slow protein−nucleic acid dissociation and stabilize complexes in the gel (*18*, *26*).

Stoichiometry experiments performed using fluorescence anisotropy and analytical ultracentrifugation indicate that up to three HU dimers bind to one 34 bp duplex and two HU dimers bind to one 13 bp duplex. These stoichiometry data suggest that the length of the DNA duplex modulates either the size of the binding site or the mode of binding. Analytical ultracentrifugation and fluorescence results yield comparable binding constants which are 3.0-fold weaker than those measured by gel shift methods (*27*). For the 13 bp duplex, all three methodologies indicate the formation of a HU_2−DNA complex. In contrast, for the 34 bp duplex the number of complexes observed by GMSA is not consistent with the number of complexes observed by fluorescence anisotropy and analytical ultracentrifugation. A relative increase (50%) in fluorescence intensity of the 34 bp duplexes is observed upon protein binding, which supports a model of induced bending. We suggest that bending of the DNA with protein binding results in a distortion of the DNA conformation, leading to a complex with significantly reduced mobility on the gel. These measurements demonstrate the relative utility of the 3-MI probe for investigating protein−DNA interactions by fluorescence anisotropy and provide an important comparison of solution and gel-based methods.

MATERIALS AND METHODS

HU Protein. HU protein was isolated from *E. coli* strain RLM1078 and purified using the following procedure (Roger McMacken, personal communication). A 300 mL cell culture with 50 μg/mL ampicillin was grown to an OD_{600} of 1.5−2.0 in Terrific broth (*28*) at 30 °C. Thermal induction was accomplished by addition of 200 mL of Terrific broth at 65 °C to the culture, yielding a final temperature of 42 °C. Cell growth was allowed to continue for 25 min at 42 °C, after which the cells were harvested by centrifugation (3000*g*; 15 min). The resulting cell pellet was rinsed with 25 mM HEPES−KOH, pH 7.6, 1 mM DTT, and 0.1 mM EDTA, resuspended in 10 mL of this buffer, and frozen. Cells were thawed at 10 °C, and 4.0 M KCl and egg lysozyme were added to final concentrations of 1.0 M and 0.25 mg/mL, respectively. After four freeze−thaw cycles, the cell lysate was centrifuged at 4 °C (100000g; 1 h). The supernatant was dialyzed against 3 × 2 L of buffer A (25 mM HEPES−KOH, pH 7.6, 50 mM NaCl, 1 mM DTT, 0.1 mM EDTA, 10% glycerol). The dialysate was loaded onto a SP-Sepharose (Amersham-Pharmacia) cation-exchange column that was developed with a 50 mM to 1.0 M NaCl linear gradient in buffer A. HU protein eluted at approximately 0.4 M NaCl. Pooled fractions were concentrated and dialyzed against buffer B (50 mM Tris-HCl, pH 7.6, 50 mM NaCl, 1 mM EDTA, 1 mM DTT, 10% glycerol) and loaded onto a DNA−cellulose column, which was prepared by UV cross-linking calf thymus DNA to cellulose (Whatman CF-11) (*29*). Protein elution was accomplished with a step gradient of 50 mM, 150 mM, 400 mM, and 2.0 M NaCl in buffer B. To eliminate a contaminating nuclease that copurifies with HU, a FPLC MonoS 5/5 cation-exchange column (Amersham-Pharmacia) was used with a 50 mM to 1.0 M NaCl gradient in buffer A. Nuclease-free HU eluted at approximately 0.35 M NaCl. The lack of nuclease activity was verified by the absence of any digested products after incubating the purified protein with plasmid DNA. HU protein concentration was determined by amino acid analysis (Keck Facility, Yale University). An extinction coefficient at 230 nm was determined to be 37.5 mM^{-1} cm^{-1}, based on seven independent analyses.

Oligonucleotides. All oligonucleotides containing the 3-MI fluorescence probe were prepared as described previously (*30*). Complementary and control oligonucleotides were purified using a 20% denaturing polyacrylamide gel. Oligo-

nucleotides were visualized by UV shadowing and eluted from the gel by copious washes with 0.3 mM sodium acetate, pH 6.5 at 37 °C, or electroelution (Schleicher and Schuell, Concord, NH). Duplex formation was achieved by mixing equal molar amounts of pure single-stranded oligonucleotides and heating at 90 °C for 5 min, followed by slow cooling to room temperature. Concentrations of single-strand oligonucleotides were determined by measuring the absorbance at 260 nm at 90 °C. Extinction coefficients were calculated using the methodology of Richards (*31*).

Steady-State Fluorescence Anisotropy and Intensity Measurements. Steady-state fluorescence anisotropy and intensity measurements were performed with a FluoroMax-2 fluorometer (Instruments SA, Metuchen, NJ). Anisotropy data were obtained using an excitation wavelength of 330 nm, and fluorescence emission was monitored from 412 to 422 nm. The integration time was 10 s/point, and data points were obtained in 3 nm increments; final values result from an average of six scans. Anisotropy values were averaged over the emission range. The average standard deviation of anisotropy measurements was ±0.0025. Fluorescence was measured at a 90° angle in an L-format. The *G*-factor was measured before each experiment and was determined to be 1.14 on average (*32*). Emission spectra were obtained from 350 to 550 nm using an excitation wavelength of 330 nm. The integration time for the intensity measurement was 1 s/point, and samples were scanned at a rate of 2 nm/point. The band-pass for both excitation and emission was 8.4 nm. Fluorescence intensity measurements were performed with the excitation polarizer set to 0° and the emission polarizer set to 55°. All samples were in a 10 mM Tris-HCl, pH 7.6, buffer containing 50 mM NaCl, 2 mM spermidine, and 0.1 mM EDTA. Samples were stirred continuously in a 3 mm × 3 mm Spectrosil S1 quartz cuvette (Starna Cells, Inc.). All measurements were done at 10 °C, and the sample temperature was maintained with a circulating bath (RTE Model 111, NESLAB Instruments, Inc.) After fluorescence experiments were performed, samples were routinely assayed using nondenaturing polyacrylamide gel electrophoresis (described below) to confirm that protein−DNA complexes had not degraded from excess light exposure.

Analysis of Binding Parameters Using Fluorescence Anisotropy. The fraction of bound DNA ($[HU_x{-}DNA]/[DNA]_T$) was determined from the fluorescence anisotropy using the relationship:

$$f = (A - A_0)/(A_\infty - A_0) \quad (1)$$

in which A, A_0, and A_∞ represent the anisotropy of the titrated sample, free DNA, and bound DNA at saturation, respectively. For experiments in which the quantum yield changes with protein binding, the anisotropy is related to f by defining the constant $R = \phi_\infty/\phi_0$, where ϕ_0 is the relative quantum yield of free DNA and ϕ_∞ is the relative quantum yield of bound DNA at saturation (*32*).

$$f = (A - A_0)/[(A_\infty - A_0)R + A - A_0] \quad (2)$$

A similar formulation was used to analyze the intensity data in which intensity measurements (i, i_0, i_∞) replace anisotropy values. Using this experimentally determined fractional saturation of the DNA and the number of HU dimers bound from the fluorescence stoichiometry and analytical ultracentrifugation experiments, the concentration of free HU ($[HU]_F$) was calculated:

$$[HU]_F = [HU]_T - fN/n \quad (3)$$

where N is the concentration of DNA in nucleotide residues and n is the binding site size (*33*, *34*). From the binding stoichiometry of 3 for the 34 bp duplexes and 2 for the 13 bp duplex, n was assumed to be 11 for the 34 bp duplex and 6 for the 13 bp duplex.

Equilibrium binding curves were fit assuming identical, noninteracting binding sites:

$$r = r_0 + \frac{nK[L](r_1 - r_0)}{1 + K[L]} \quad (4)$$

where r, r_0, and r_1 represent the anisotropy of the titrated sample, free DNA, and DNA with one HU protein bound, respectively. K is the microscopic binding constant, and n represents the number of ligands bound. In this formulation the fractional change in anisotropy was considered equal for each binding event (*35*). [L] corresponds to the concentration of free ligand, in this case HU protein. In these analyses, n was held constant and determined independently by fluorescence anisotropy and analytical ultracentrifugation measurements. The above equation was modified to take into account the change in fluorescence intensity upon binding:

$$r = \frac{r_0(1 + K[L]) + nK[L](Rr_1 - r_0)}{1 + K[L] + nK[L](R - 1)} \quad (5)$$

where $R = \phi_1/\phi_0$ and ϕ_1 = the fluorescence yield after binding the first ligand. Equilibrium binding constants were evaluated using the Marquardt−Levenberg least-squares algorithm and the appropriate equations within the program Origin 6.0 (Microcal). Quality of the fit was evaluated by visual inspection, χ^2 values, and the correlation coefficients.

Gel Mobility Shift Assays. Gel mobility shift or gel retardation assays were performed on HU protein complexed with the oligonucleotides shown in Table 1. A 6.5% nondenaturing acrylamide gel was prepared in 22.5 mM Tris base, 22.5 mM boric acid, and 0.625 mM EDTA (TBE). Samples were prepared in a 10 mM Tris-HCl, pH 7.6, buffer containing 50 mM NaCl, 2 mM spermidine, 0.1 mM EDTA, and 10% glycerol and were incubated for 20 min at room temperature before being loaded onto the gel (*12*). Gels were prerun at 10 V/cm for 1 h or until the current had stabilized. Samples were loaded at a constant voltage of 10 V/cm and after 5 min of migration, the voltage was reduced to 8.5 V/cm at 4 °C. DNA-containing bands were visualized using the fluorescent dye Syber Green (Molecular Probes, Eugene, OR). Fluorescent bands were analyzed using Storm Imager 840 (Molecular Dynamics, Inc.) and quantified using Image Quant Version 4.2 (Molecular Dynamics, Inc.). For the analyses, boxes defining bound DNA extended from the free DNA to the slowest migrating complex. Therefore, the concentration of bound DNA is determined from the summed intensities of all the complex bands observed in a single lane of the gel. The background was defined from a similar box in a lane, which did not contain any protein. Apparent dissociation constants, K_d(app), were determined by assuming

a one-to-one binding interaction using the equations:

$$K_d(\text{app}) = [\text{HU}][\text{DNA}]/[\text{DNA}-\text{HU}_x] \quad (6)$$

and

$$f = [\text{DNA}-\text{HU}_x]/[\text{DNA}]_T \quad (7)$$

Substitution of (7) into (6) and rearrangement yield the binding equation:

$$f = \{([\text{HU}]_T + [\text{DNA}]_T + K_d) - \sqrt{([\text{HU}]_T + [\text{DNA}]_T + K_d)^2 - 4[\text{DNA}]_T[\text{HU}]_T}\}/2[\text{DNA}]_T \quad (8)$$

In eq 8, K_d refers to an apparent K_d as described above. Optimization of binding parameters was performed using the nonlinear least-squares fitting package from Origin 6.0 (Microcal).

Analytical Ultracentrifugation. HU protein and DNA were exchanged into a 10 mM Tris, pH 7.6, buffer containing 50 mM NaCl, 15 mM KCl, 2 mM spermidine, and 0.1 mM EDTA using Bio-Rad Biospin 6 spin columns. Analytical ultracentrifugation measurements were performed with six-channel (1.2 cm path) charcoal−epon cells with a Beckman XL-I centrifuge and an An-60Ti rotor at a temperature of 4°. Samples of 110 μL volume were loaded on top of 10 μL of FC-43 fluorocarbon. Scans were recorded at 230 and 260 nm using 0.001 cm point spacing and averaging 10 readings at each point. Equilibrium was judged to be achieved by the absence of systematic deviations in a plot of the difference between successive scans taken 6 h apart. For HU protein, $\bar{\nu}$ was calculated from the amino acid composition to be 0.739 mL/g at 4 °C. Data were fit using the Marquardt−Levenberg least-squares algorithm using macros written within the IGOR Pro (Wavemetrics, Inc.) package. Buoyant molecular weights for HU and DNA were determined by fitting data to the single ideal species model and are tabulated as follows, along with the measured extinction coefficients used in the global data analysis.

component	M_{buoyant}	ϵ_{230} (mM^{-1} cm^{-1})	ϵ_{260} (mM^{-1} cm^{-1})
HU	4994	37.5	2.40
H1-13-CT	4507	9.35×10^2	2.45×10^2
H1-34-CT	10061	2.38×10^2	6.23×10^2

Weight-average buoyant molecular weights were obtained by fitting the 260 nm data to the expression:

$$A(r) = \delta + A_0 e^{\bar{M}M_{w,B}\xi}$$

where $A(r)$ is the DNA absorbance at distance r, δ is a baseline offset, A_0 is the absorbance at the reference distance r_0, $M_{w,B}$ is the weight-average buoyant molecular weight, and $\xi = (r^2 - r_0^2)\omega^2/2RT$, where ω is the angular velocity. Note that at 260 nm the molar extinction coefficient of HU is less than 1% relative to the DNA duplex, so the protein absorbance does not contribute significantly to the signal.

Global analysis was performed by fitting to the association model:

$$A_{r,\lambda} = \delta_\lambda + \epsilon_{\lambda,P}C_{0,D}e^{M_D\xi} + \epsilon_{\lambda,P}C_{0,P}e^{M_P\xi} + \sum_{i=1}^{N}(\epsilon_{\lambda,D} + i_{\epsilon\lambda,P})C_{0,D}(C_{0,P})^i e^{\sum_{i=1}^{N}(\ln K_i)}e^{(M_D+iM_P)\xi}$$

where $A_{r,\lambda}$ is the absorbance at radius r and wavelength λ, δ_λ is the baseline offset at wavelength λ, $\epsilon_{\lambda,D}$ is the molar extinction coefficient of DNA at wavelength λ, $C_{0,D}$ is the molar concentration of free DNA at the reference distance r_0, M_D is the buoyant molecular weight of the DNA, and N is stoichiometry of HU binding. Symbols with the subscript P refer to the protein and are defined analogously. Control experiments demonstrated that the extinction coefficients did not change appreciably upon complex formation. For the H1-13-CT experiments, the DNA concentration was held constant at 1 μM with HU concentrations of 0.5, 1, 2, and 5 μM and rotor speeds of 25 000 and 30 000 rpm. For H1-34-CT, the DNA concentration was 0.25 μM, with HU concentrations of 0.25, 0.5, 1, and 2 μM at rotor speeds of 15 000 and 20 000 rpm. Data were recorded at 230 and 260 nm, giving a total of 16 data channels for each DNA sequence.

RESULTS

Fluorescence Properties of 3-MI Oligonucleotides. HU binding to linear DNA was investigated using oligonucleotides of 13 and 34 bp (Table 1) to determine the nature of the binding site and the DNA conformational changes that occur upon protein binding. Since the HU protein has no naturally occurring fluorophores such as Trp or Tyr, fluorescence changes upon protein binding were monitored through DNA oligonucleotides containing the fluorescent probe 3-methyl-8-(2-D-ribofuranosyl)isoxanthopterin (3-MI) (*30*) (Figure 1). Oligonucleotides containing the 3-MI probe are structurally and energetically similar to control DNA duplexes. Optical absorption thermal melting experiments reveal that T_m values determined for 3-MI containing oligonucleotides are depressed by 4° relative to oligonucleotides of the same sequence that do not contain the 3-MI probe (data not shown). The decrease in T_m is comparable to that observed for DNA duplexes containing one mismatch and is reflective of the fact that the 3-MI probe can stack with other DNA bases but does not form H-bonds (*36*).

Using an excitation wavelength of 330 nm, the 3-MI monomer is very fluorescent in solution with a measured quantum yield $\Phi = 0.88$ relative to quinine sulfate (*30*) (Figure 1). The fluorescence quantum yield of the 3-MI probe is extremely sensitive to local environment, and incorporation of 3-MI into a DNA strand results in a significant reduction in fluorescence intensity. The fluorescence quantum yield relative to the 3-MI monomer decreases to 0.23 for the H1-34-2 oligonucleotide and further decreases to 0.08 upon duplex formation. In the case of the H1-34-1 oligonucleotide, duplex formation causes the relative quantum yield to decrease to 0.04 (Figure 1). The composition of bases adjacent to the probe strongly influences the observed fluorescence yield; 3-MI is located between two adenosine residues in the H1-34-1 oligomer and an adenosine and a thymine in the H1-34-2 oligomer (Table 1). Maximal quenching was previously detected when the 3-MI probe was adjacent to adenosine residues (*30*); therefore, the decreased

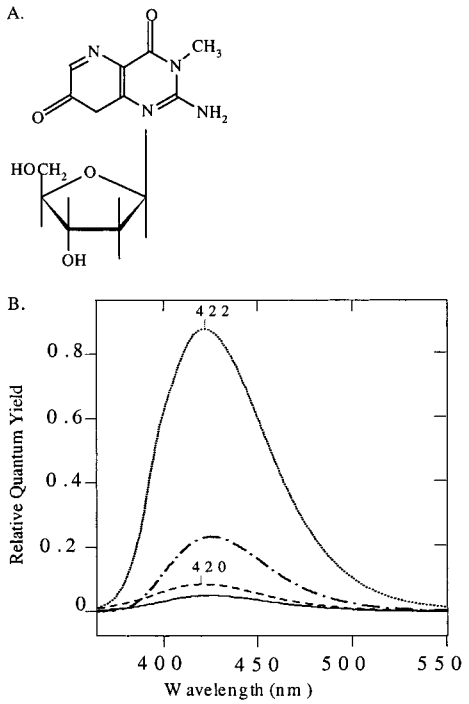

FIGURE 1: (A) Chemical structure of 3-methyl-8-(2-deoxy-β-D-ribofuranosyl)isoxanthopterin (3-MI). (B) Fluorescence spectrum of the 3-MI monomer (···) and the spectra when incorporated into a 34 bp single strand, H1-34-2 (— · —), and a duplex, H1-34-2 (---) and H1-34-1 (—). Excitation at 330 nm results in a maximum emission of 422 nm for the monomer, single strand, and duplex. Quantum yields shown are relative to the 3-MI monomer. Note that, upon duplex formation, the quantum yield is significantly quenched, 100-fold for H1-34-2 and 200-fold for H1-34-1. Samples were in a 10 mM Tris, pH 7.6, buffer containing 50 mM NaCl, 2 mM spermidine, and 0.1 mM EDTA.

fluorescence quantum yield measured for the H1-34-1 duplex relative to the H1-34-2 duplex is consistent with previously determined quenching patterns.

Stoichiometry of HU−DNA Complexes. In previous HU binding studies multiple complex formation was observed by the gel mobility shift assay technique (GMSA); therefore, we have investigated the stoichiometry of HU binding to DNA by analytical ultracentrifugation and fluorescence anisotropy methods. Control oligonucleotides (H1-13-CT; H1-34-CT) that did not contain the 3-MI probe were used in the sedimentation equilibrium experiments, whereas 3-MI-containing oligonucleotides (H1-13-1; H1-34-1) were used in fluorescence stoichiometry measurements.

First, the HU heterodimer was characterized in the absence of DNA. Data obtained at 2.6, 4.9, and 9.9 μM protein at 20 000, 25 000, and 30 000 rpm were globally fit to a single ideal species model with a best-fit mass of 18 480 (18 020−18 950) (values in parentheses are two standard deviation confidence intervals). Within experimental error, this value corresponds to the mass expected for the HU heterodimer (18 755), indicating that HU exists as a stable, homogeneous dimer over this concentration range. Similarly, the control DNA duplexes, H1-13-CT and H1-34-CT, were found to exist as homogeneous species (data not shown).

The stoichiometry of the HU−DNA complexes was determined by titrating H1-13-CT or H1-34-CT DNA with increasing concentrations of HU and detecting the increase in the weight-average buoyant molecular weight of the DNA at 260 nm. Since HU has no Trp residues, at this wavelength there is essentially no contribution from the free HU in solution. In the presence of excess HU, the DNA should become saturated and the weight average molecular weight asymptotically approaches the buoyant mass of the saturated HU_x−DNA complex. As shown in Figure 2, for both oligomers the buoyant molecular weight increases with HU concentration, consistent with protein binding to DNA. The amplitude of the increase is consistent with two HU proteins binding to H1-13-CT and more than two HU proteins binding to H1-34-CT.

The stoichiometry of binding was further verified using fluorescence anisotropy. This was accomplished by titrating HU into a solution of either H1-13-1 or the H1-34 duplexes at a concentration 10-fold greater than the K_d. At this relatively high concentration of binding sites, the DNA binds all of the added HU protein. Consequently, the anisotropy as a function of the molar ratio of HU:DNA should yield a clear inflection point, indicating the binding stoichiometry (*21*, *37*). For the H1-13-1 duplex a distinct inflection point is observed and occurs at approximately two HU dimers to one 13 bp duplex (Figure 3). For the H1-34-1 duplex the inflection point is not so clearly defined; however, the linear binding and plateau regions can be extrapolated to give a binding stoichiometry of greater than two HU dimers to one 34 bp duplex (Figure 3).

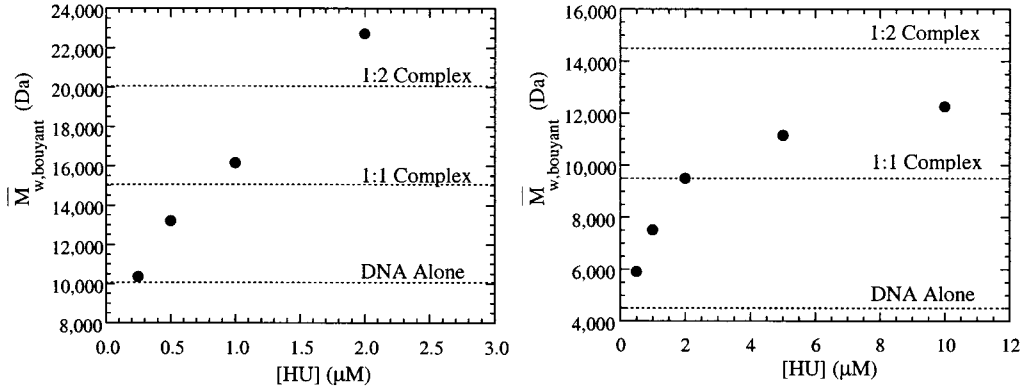

FIGURE 2: Determination of HU binding stoichiometry using equilibrium analytical ultracentrifugation. (Left) Binding of HU to the control 34 bp duplex, H1-34-CT. DNA (0.25 μM) was titrated with increasing concentrations of HU, and the weight-average buoyant molecular weight was determined as described in the Materials and Methods section at a rotor speed of 15 000 rpm. Dotted lines indicate expected masses for DNA alone and 1:1 and 1:2 complexes with HU. (Right) Binding of HU to the control sequence of the 13 bp duplex, H1-13-CT. The DNA concentration is 1 μM, and the rotor speed is 25 000 rpm.

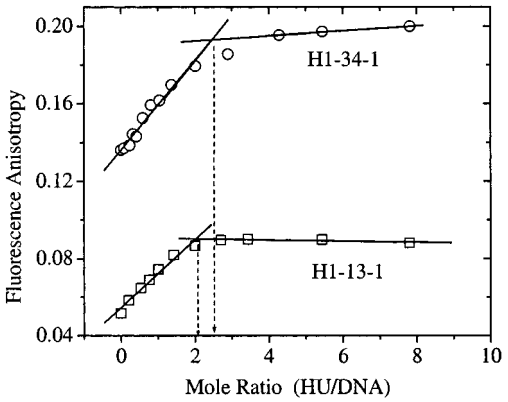

FIGURE 3: Determination of stoichiometry using fluorescence anisotropy from H1-34-1- and H1-13-1-bound HU complexes. The intersection from the crossover of the slope and the plateau indicates the saturated molar ratio of HU to DNA for that oligomer. (○) H1-34-1 yields a molar ratio of up to three HU molecules per DNA. (□) H1-13-1 yields a molar ratio of 2 HU molecules.

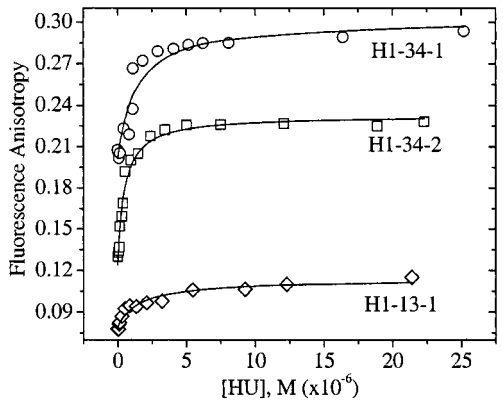

FIGURE 4: DNA binding affinity of HU to 34 and 13 bp oligonucleotides determined by fluorescence anisotropy. The experimental data are fitted to eqs 4 and 5 as described in the Materials and Methods section. (○) H1-34-1: for clarity, r shown = r values + 0.06; $K_a = 0.50\ \mu M^{-1}$; $\Delta r = 0.086$; [DNA] = 0.8 μM. (□) H1-34-2: $K_a = 0.71\ \mu M^{-1}$; $\Delta r = 0.098$; [DNA] = 0.8 μM. (◇) H1-13-1: $K_a = 0.72\ \mu M^{-1}$; r shown = r values + 0.04; $\Delta r = 0.033$; [DNA] = 0.3 μM.

The bending of the DNA induced upon protein binding, as suggested by the fluorescence intensity measurements (vide infra), leads to a change in shape that would increase the rotational diffusion of the sample. This increase in rotational diffusion results in a decrease in anisotropy. Therefore, we propose that the slightly lower than 3:1 binding stoichiometry obtained by anisotropy occurs because of the change in shape of the protein−DNA complex; however, the most likely HU:DNA ratio is 3:1. Thus, by both analytical ultracentrifugation and fluorescence anisotropy we have determined that two HU dimers bind to the 13 bp duplex DNA and three HU dimers bind to the 34 bp duplex DNA.

Equilibrium Binding of HU to DNA

(A) Fluorescence Anisotropy. HU binding to DNA results in an increase in molecular size and a change in shape, leading to a decrease in rotational correlation time and an increase in fluorescence anisotropy. Figure 4 depicts HU binding to 13 and 34 bp duplexes as monitored by fluorescence anisotropy. As expected, in the absence of HU, the smaller size of the 13 bp duplex results in a lower initial anisotropy value relative to the 34 bp duplex (0.04 vs 0.12, respectively). The H1-34 duplexes also experience a larger change in anisotropy ($\Delta r \sim 0.10$) as a consequence of protein binding whereas for H1-13-1 the total anisotropy change ($\Delta r = 0.036$) is approximately one-third of the 34 bp oligomers. This is consistent with the larger size of the 34 bp duplex and the greater HU:DNA binding stoichiometry. The overall anisotropy change may in fact be reduced by an increase in lifetime upon binding. The relationship between correlation time (ϕ) and lifetime (τ) is shown in the form of the Perrin equation:

$$\bar{r} = \frac{\bar{r}_0}{1 + \bar{\tau}/\bar{\phi}}$$

In the case of the two duplexes without protein, the observed anisotropy differences are solely related to the difference in ϕ. Similarly, the absence of a fluorescence intensity change upon HU binding to H1-13-1 is suggestive that the lifetimes are constant and the anisotropy changes are solely related to differences in ϕ. We cannot rule out the possibility, however, that changes in τ may accompany protein binding to the H1-34 duplexes, which lead to a smaller overall anisotropy change.

For all three duplexes, protein binding initially leads to an increase in anisotropy, which plateaus at protein concentrations greater than 3 μM. In contrast to the stoichiometry studies, for these measurements the DNA concentration was held constant at a value close to or below the dissociation constant (<1 μM). These saturable binding curves can be used to determine the equilibrium binding constant for the interaction between HU and the 3-MI oligomers (Table 2) (*21*−*23*). The data shown are fit to a model of noninteracting binding sites, in which the number of binding sites was determined from the stoichiometry data (Figure 4) (*35*). For H1-34-1 and H1-34-2, the determined microsopic association constants (k) are well within error of each other and are approximately 0.6 μM^{-1}. These microscopic binding constants are related to the stepwise binding constants, such that $K_1 = 3k$, $K_2 = k$, and $K_3 = k/3$ (Table 2). As these oligomers differ only in the placement of the probe, the similarity in binding constant indicates that the position of the 3-MI probe within the DNA duplex does not significantly perturb HU binding. Binding to the H1-13-1 duplex is also well described by an independent binding site model, which yields a microscopic association constant of 0.62 μM^{-1} (Table 2). Since only two HU dimers bind to H1-13-1, in this case $K_1 = 2k$ and $K_2 = k/2$. Within error these association constants are indistinguishable, which suggests that the apparent binding affinity of HU to these relatively short pieces of DNA is independent of duplex length.

(B) Fluorescence Intensity. At HU concentrations below 4 μM, protein binding leads to an increase in fluorescence intensity of the H1-34 duplexes (Figure 5). Both duplexes exhibit a fluorescence intensity increase of 50% relative to the initial values. Since the fluorescence yield of the 3-MI probe is so sensitive to local environment and stacking interactions (Figure 1), the relative increase in fluorescence intensity observed with protein binding probably results from a reduction in stacking interactions that leads to an increase in solvent exposure of the probe. These effects are suggestive of a local unwinding or bending of the DNA helix upon HU

Table 2: Equilibrium Binding Constants Determined for HU

DNA duplex	anisotropy (μM^{-1})[d]	intensity (μM^{-1})[d]	GMSA (μM^{-1})[e]	sedimentation equilibrium (μM^{-1})
H1-34-1[a]	0.50 ± 0.27 ($n = 3$)	0.88 ± 0.42 ($n = 3$)	1.23 ± 0.12	
H1-34-2[a]	0.71 ± 0.10 ($n = 3$)	0.77 ± 0.33 ($n = 3$)	2.44 ± 0.24	
H1-34-CT[b]			1.99 ± 0.20	0.57 ± 0.11 ($n = 3$)
H1-13-1[a]	0.72 ± 0.14 ($n = 2$)	N/A		
H1-13-CT[c]				0.35 ± 0.03 ($n = 2$)

[a] Sequences as shown in Table 1. [b] H1-34-CT represents a control 34 base pair duplex, which has the same sequence as H1-34-1 and H1-34-2 but does not contain the 3-MI fluorescent probe. [c] H1-13-CT represents a control 13 base pair duplex, which has the same sequence as H1-13-1 but does not contain the 3-MI fluorescent probe. [d] Data were fit using an identical, noninteracting or independent binding site model. The number of sites was determined independently from fluorescence stoichiometry and analytical ultracentrifugation experiments. For the H1-34 duplexes, $n = 3$ and the stepwise binding constants are $K_1 = 3k$, $K_2 = k$, and $K_3 = k/3$, where k is the microscopic association constant given in the table. For the H1-13-1 duplex, $n = 2$ and the stepwise binding constants are $K_1 = 2k$ and $K_2 = k/2$, where k is the microscopic association constant given in the table. [e] A K_a(app) is reported for the GMSA, as the entire concentration of bound complexes is considered in the analysis.

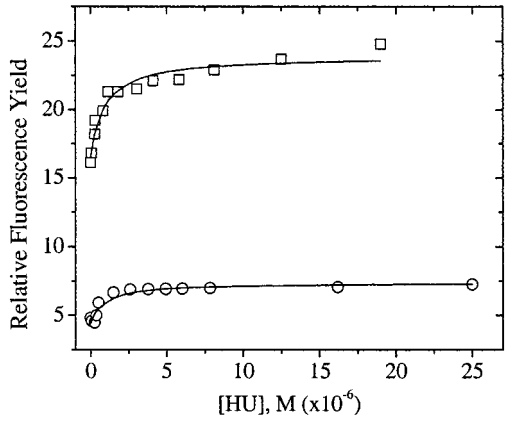

FIGURE 5: DNA binding affinity of HU to the H1-34-1 and H1-34-2 oligonucleotides determined by fluorescence intensity. A K_a of 0.88 μM^{-1} for H1-34-1 (○) and 0.77 μM^{-1} for H1-34-2 (□) is obtained from fitting the data to eq 4. Experimental conditions are the same as those of the anisotropy experiment. Samples were excited at 330 nm while fluorescence emission was monitored at 416 nm with the excitation polarizer set to 0° and the emission polarizer set to 55°.

binding, as substantial quenching of 3-MI fluorescence is observed in single-stranded oligonucleotides. No change in fluorescence intensity is observed upon HU binding to the H1-13-1 duplex. In this case the shorter length of the duplex probably prohibits the deformation detected for the 34 bp duplexes.

The difference in the fluorescence intensity change of the H1-34 duplexes upon protein binding is attributed to the degree of quenching caused by the nucleic acid bases adjacent to the 3-MI probe. The H1-34-1 oligonucleotide is quenched to a greater extent in both the single- and double-stranded forms (Figure 1); therefore, the magnitude of the intensity increase upon protein binding is not as great as for the H1-34-2 duplex. Nevertheless, the relative intensity increase is comparable for both H1-34 duplexes, indicating that a similar mode of interaction with the protein is occurring.

The increase in fluorescence intensity detected as a function of HU concentration exhibits saturable binding (Figure 5) similar to that observed with fluorescence anisotropy. Analysis of the curves with the independent binding site model yields microscopic association constants of ~0.82 μM^{-1} that are in good agreement with those determined by fluorescence anisotropy (Table 2). The relative similarity in the equilibrium association constants determined for both the intensity and the anisotropy measurements for the 34 bp duplexes is suggestive of bending accompanying HU binding to DNA. Since a fluorescence intensity change is not observed for the 13 bp duplex, bending of DNA does not necessarily accompany HU binding. Further, the relative comparabilities of the equilibrium association constants for the 13 and 34 bp duplexes (Table 2) are suggestive that induced bending of DNA does not affect HU binding affinity.

(C) Analytical Ultracentrifugation. The equilibrium constants for HU binding to each DNA were determined by globally fitting 16 data sets recorded at 230 and 260 nm with multiple concentrations of HU and DNA to the appropriate association models (Table 3). For H1-13-CT, good fits were obtained for a model in which two HU proteins bind with equal association constants (Figure 6). A slightly worse fit is obtained if the statistical factors are included in the model. If the two association constants are fitted independently, the fit is slightly improved, but within experimental error the two association constants are barely distinguishable. For H1-34-CT, the data fit well to a model involving three HU proteins binding with equal affinity to the DNA, and again, a slightly worse fit is obtained if the statistical factors are included. These data indicate that binding of HU to these linear DNA duplexes is not highly cooperative and possibly exhibits very weak positive cooperativity.

The equilibrium binding constants determined by analytical ultracentrifugation, fluorescence anisotropy, and intensity are in excellent agreement (Table 2). We further note that the analytical ultracentrifugation experiments were performed on control or non-3-MI-containing duplexes; therefore, these measurements demonstrate that the presence of 3-MI in the duplexes does not perturb the HU−DNA binding interaction. In addition, the shape of the binding curve as determined by all three methods is indicative of a binding interaction, which exhibits little to no cooperativity.

(D) Gel Mobility Shift Assay. Gel mobility shift assays were performed to further verify that the binding of HU to DNA was not perturbed by the presence of the 3-MI fluorescence probe. In these assays binding experiments were performed with control (data not shown) and 3-MI-containing oligomers (Figure 7). Experiments were performed with a constant concentration of DNA (0.4 μM) and increasing concentrations of HU, ranging from 0.0001 to 10 μM. At molar ratios of HU:DNA of 0.5 and higher (lanes 7−14), two and three complexes are seen on the gel. Concentrations of HU greater than 1 μM lead to the observation of

Table 3: Equilibrium Constants for HU−DNA Binding Determined by Analytical Ultracentrifugation

model	ln K_1[a]	ln K_2	RMS[b]
H1-13-CT			
$A + 2B \rightarrow AB_2$, $K_2 = K_1$	12.77 (12.68, 12.87)		0.00816
$A + 2B \rightarrow AB_2$, $K_1 = 2k$, $K_2 = k/2$	13.52 (13.41, 13.60)	12.13	0.00877[c]
$A + 2B \rightarrow AB_2$	12.38 (11.79, 12.85)	13.14 (12.97, 13.31)	0.00809
H1-34-CT			
$A + 3B \rightarrow AB_3$, $K_1 = K_2 = K_3$	13.26 (13.07, 13.46)		0.00758
$A + 3B \rightarrow AB_3$, $K_1 = 3k$, $K_2 = k$, $K_3 = k/3$	14.61		0.00813[d]

[a] Natural logarithm of the molar association constants. Values in parentheses refer to the one standard deviation joint confidence intervals. [b] Root mean square deviation in OD units. [c] For two independent and equivalent sites, $K_1 = 2k$ and $K_2 = k/2$, where k refers to the microscopic association constant. $\ln K_2 = \ln K_1 - \ln 4 = 12.13$. [d] For three independent and equivalent sites, $K_1 = 3k$, $K_2 = k$, and $K_3 = k/3$, where k refers to the microscopic association constant. $\ln K_2 = 13.60$, and $\ln K_3 = 12.50$.

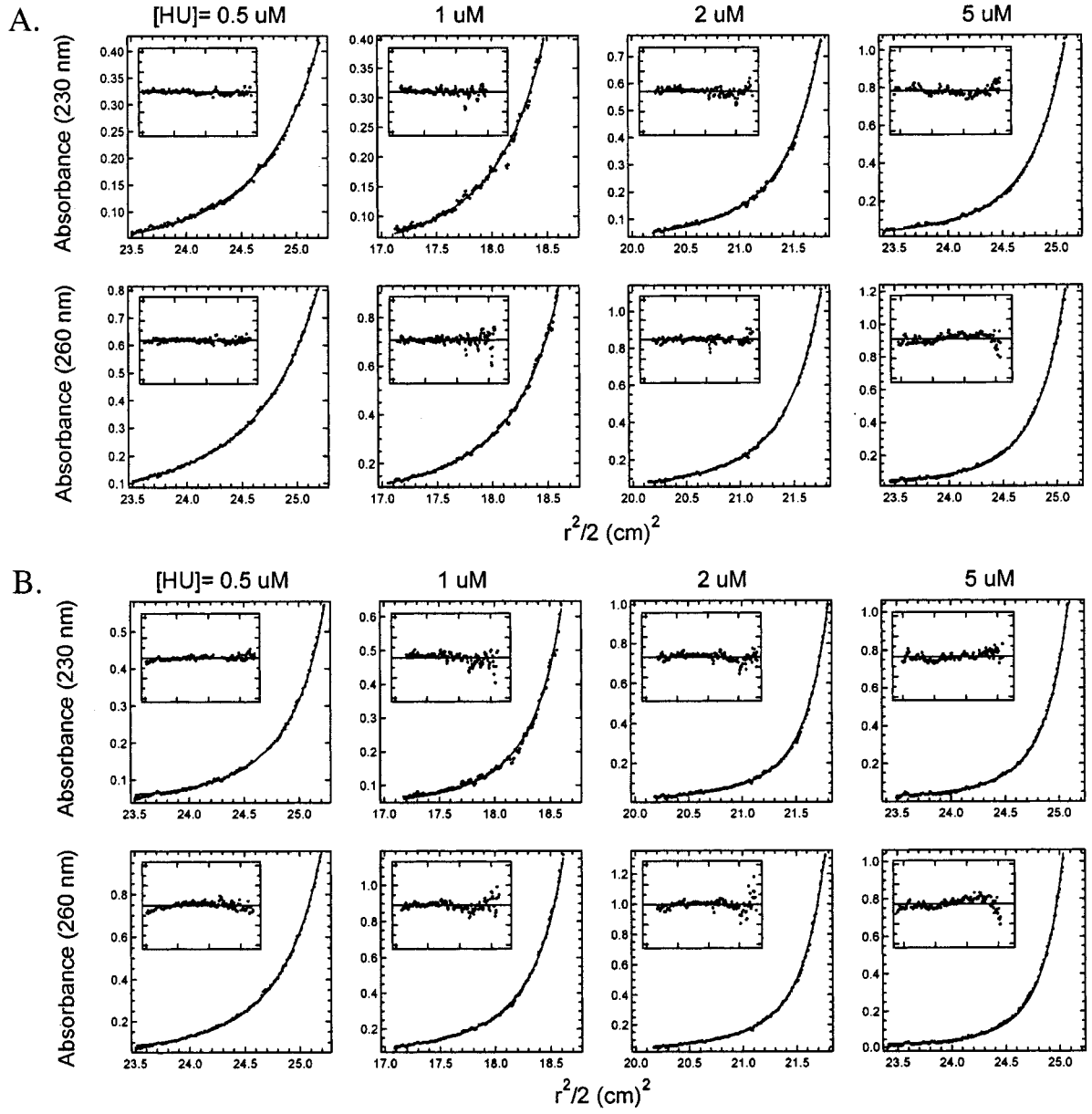

FIGURE 6: Analysis of sedimentation equilibrium of HU binding to H1-13-CT: (A) rotor speed of 25 000 rpm; (B) rotor speed of 30 000 rpm. The concentration of H1-13-CT is 1 μM. The data are indicated as points, and the solid lines are the global fit of all 16 channels to the model in which the two association constants are allowed to vary independently. The insets show the residuals, with a scale from −0.08 to 0.08 OD. The results of the fit are given in Table 3.

complexes with very reduced mobility on the gel. The observation of these bands is correlated with the disappearance of free DNA and faster migrating complexes. In previous experiments the observation of similar bands was interpreted to be indicative of several HU dimers binding to a linear piece of DNA (*12*).

For the H1-34 duplexes, up to five distinct complexes can be observed on the gel (Figure 7A), and the strong intensity

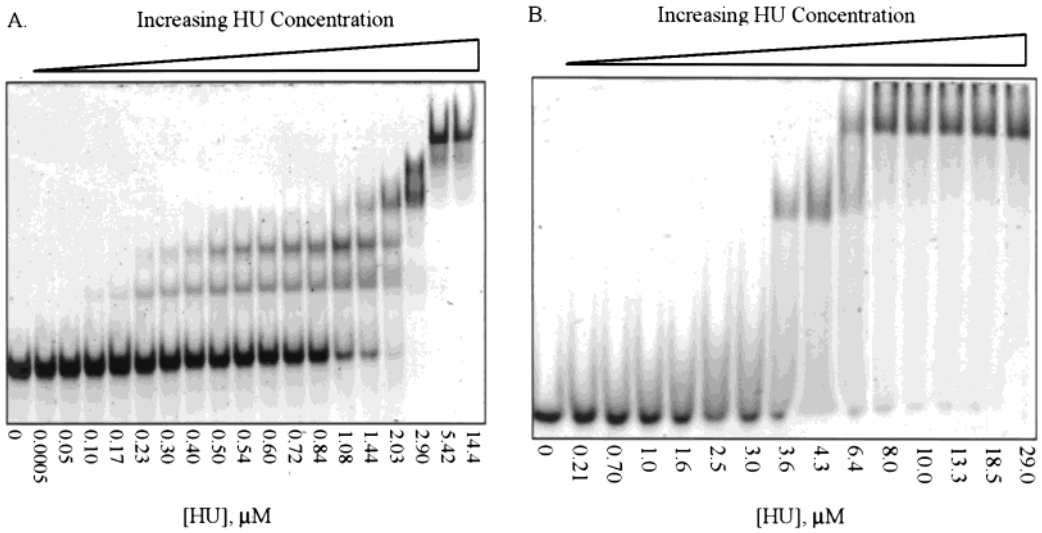

FIGURE 7: Gel mobility shift assay of HU binding to selected duplexes. (A) HU binding to H1-34-1. The total DNA concentration was constant at 0.45 μM. The slight decrease in migration of free DNA is a result of loading the gel at high voltage. A K_a(app) of 1.23 μM^{-1} was obtained from fitting the experimental data to eq 8. (B) HU binding to H1-13-CT. The DNA concentration was constant at 0.4 μM.

of the bands is indicative of relatively stable complexes. In the GMSA, the H1-34 duplexes exhibit a small but appreciable difference in their equilibrium binding constants, where the K_a(app) of H1-34-2 is twice that of H1-34-1 (Table 2). The determined binding constants are 3-fold stronger than those determined by fluorescence anisotropy and equilibrium sedimentation. The GMSA-determined equilibrium binding constants for H1-34-2 and H1-34-CT are in good agreement with the binding constant previously determined for HU binding to linear DNA by GMSA (*12*, *27*). Therefore, the increased affinity of HU in the gel relative to the solution-based measurements (see above) is attributed to the caging effect and sequestration induced by the medium (*26*, *38*). These effects can lead to reduced dissociation rate constants and enhanced bimolecular reassociation, which may act to stabilize the protein−DNA complexes in the gel (*26*).

In contrast to the 34 bp duplexes, the 1:1 complex formed by the H1-13-1 duplex is difficult to observe due to relatively fast dissociation (Figure 7B). However, the broad smear observed (lanes 2−7) may be indicative of 1:1 complex formation. Stable 1:1 HU−DNA complexes are only observed at protein concentrations greater than 4.3 μM, at which point 2:1 HU−DNA complexes are beginning to be observed. The relatively fast dissociation of the 13 bp HU−DNA complex prevents an accurate determination of the binding constants using GMSA.

DISCUSSION

Size of the HU Binding Site. In earlier studies of HU binding nonspecifically to linear DNA duplexes and supercoiled DNA, the binding site size was measured to be approximately 9 bp (*9*, *12*). This value was consistent with a linear model of HU dimers binding to DNA originally proposed by Tanaka and co-workers (*3*). If the linear binding model is assumed, the ultracentrifugation and anisotropy stoichiometry data suggest that the binding site size changes with duplex length. Specifically, a 6.5 bp binding site is predicted for the 13 bp duplex, while an 11 bp binding site is implicated for the 34 bp duplex. For the 13 bp duplex, a 9 bp binding site cannot be accommodated by a linear binding model, and this size binding site is only possible if alternate binding modes or protein−protein interactions induced by DNA binding are invoked to lead to the observed stoichiometry. The lack of an observed fluorescence intensity change in H1-13-1 with protein binding is supportive of an alternate binding mode for the 13 bp duplex relative to the 34 bp duplexes. For the H1-34 duplexes used in this study, a 9 bp binding site predicts that three HU molecules bind with a spacing of 2−3 bp. In an earlier binding study that examined a 37 bp duplex containing four nucleotide loops, optimal HU binding occurred when the loops were spaced at 8−9 bp intervals. In that study, the loops were thought to confer additional flexibility and bending to the DNA sequence (*39*). A 9 bp binding site is appealing since this spacing was observed between the two intercalated tips of the β arms in the IHF−DNA cocrystal structure (*7*). In the GMSA data, if the number of HU proteins bound is equated to the number of bands observed, the linear binding site model predicts a smaller binding site of ~7 bp for both the 34 and 13 bp duplexes. In summary, these data are strongly suggestive that either the binding site size or the mode of binding is altered upon HU binding to the 13 bp duplex.

Cooperativity of HU Binding. The best fits to the binding curves (Figures 4 and 5) were obtained when an identical, noninteracting or independent binding site model was used. In this model, all sites are equivalent, and the microscopic association constant describes the binding affinity. As the number of binding sites was independently determined from the stoichiometry data, this parameter was held constant.

Nevertheless, the nonspecific nature of HU binding argues for consideration of the potential number of binding sites on each duplex. Therefore, we have also examined the equilibrium binding curves using the nonspecific binding model for protein−DNA interactions developed by von Hippel and co-workers (*33*). The equilibrium fluorescence anisotropy and intensity data were evaluated by considering both the cooperative and noncooperative case of binding. For these analyses, the binding site size was inferred from the binding stoichiometry and taken to be 11 for the 34 bp duplex and 6 for the 13 bp duplex. For the noncooperative

case, nonlinear least-squares fitting yielded binding constants which were in good agreement with those determined by the independent binding site model (data not shown). We were, however, unable to obtain good simulations of the binding data assuming cooperativity. These results do not completely rule out the possibility of a weakly cooperative binding interaction with an ω value of ≤ 10 in solution. We note that neither the cooperative nor the noncooperative binding model, which was originally formulated for the infinite lattice, describes the data as well as the noninteracting binding site model (Figures 4 and 5). This is not surprising considering the length of the duplexes used in this study. These analyses support the finding that HU binding to DNA is not highly cooperative but may exhibit weak positive cooperativity. Previously, reports of HU binding to linear DNA as measured by GMSA had found that the binding was cooperative (*16*, *40*). This cooperativity, which is stronger than that measured in the current study, probably arises in part from the caging effect of the gel, which also results in a stronger binding constant compared to the solution data (Table 2).

Nonspecific Binding and Protein-Induced Bending. The sequences of the duplexes (Table 1) used in this study are based upon the H1 binding site of IHF. IHF recognizes a specific DNA sequence (underlined in Table 1), binds to ~35 bp, and introduces a >160° bend (*7*, *8*). Both HU and IHF are members of a family of histone-like proteins, and the two proteins are nearly identical with respect to primary and secondary structure (*5*−*8*). Although HU typically binds to DNA nonspecifically, in the presence of integrase (Int), HU binds to the H1 sequence with high affinity and specificity, forming an intasome (*20*). Comparable HU binding specificity has also been observed in higher order nucleoprotein structures, such as the gal repressor complex (*41*) and the Mu transpososome (*13*, *14*). HU binding to nicked (*17*), cruciform (*15*, *16*), and negatively supercoiled DNA (*19*) exhibits similar binding specificity. Conversion of HU to a chemical nuclease has shown that the mode of binding in these nucleoprotein structures is similar to that of IHF (*14*, *18*, *41*). In the current study HU binding to linear DNA is considerably weaker and differs markedly from that observed for these specialized DNA conformations. These measurements directly show that sequence alone is not sufficient for specificity in the HU−DNA interaction, as only weak binding to the H1 sequence was detected while specific complexes were observed in the presence of the Int protein (*20*). Thus, the conformation of the DNA or the presence of additional factors, which may facilitate loop formation, gives rise to a more specific HU−DNA interaction. Consistent with the results from other studies (*19*), these observations suggest that the specificity in binding arises from DNA conformation.

In the current study bending or unwinding accompanies HU binding, as shown by the relative increase in fluorescence intensity and the similarity in binding constants determined by fluorescence anisotropy and intensity. Therefore, we note that HU may also induce a bend when binding to linear DNA nonspecifically, as does the functionally similar HMG protein (*42*).

For the 34 bp duplexes potentially five HU−DNA complexes are observed by GMSA; however, the stoichiometry as determined by other methods indicates that only three HU dimers bind to one 34 bp duplex. These solution binding and stoichiometry data argue for a revised interpretation of the GMSA data. We propose that the additional complexes observed in the gel result from different protein-induced conformations of the bound DNA (Figure 7). Protein-induced DNA bending leads to the formation of complexes which have different mobilities in the gel but the same stoichiometric ratio of HU:DNA. This binding and induced bending are consistent with the function of HU as an architectural protein. Given the relatively high concentrations of HU in the cell, we speculate that both nonspecific and specific binding interactions are of functional significance.

In summary, the excellent agreement between the sedimentation and fluorescence binding results demonstrates that fluorescence measurements performed with the 3-MI probe are an effective method for monitoring protein−DNA interactions in solution. Fluorescence intensity measurements further suggest that bending of linear DNA accompanies HU binding. These solution equilibrium binding data are well described by a noninteracting binding site model, indicating little to no cooperativity. Further experiments are needed to characterize the complexes in the gel and to evaluate HU binding affinity for bent or looped structures in solution.

ACKNOWLEDGMENT

We thank Prof. Roger McMacken for the gift of the RLM1078 *E. coli* strain and for helpful advice regarding HU isolation and purification.

REFERENCES

1. Drlica, K., and Rouviere-Yaniv, J. (1987) *Microbiol. Rev. 51*, 301−319.
2. Bewley, C. A., Gronenborn, A. M., and Clore, G. M. (1998) *Annu. Rev. Biophys. Biomol. Struct. 27*, 105−131.
3. Tanaka, I., Appelt, K., Dijk, J., White, S. W., and Wilson, K. S. (1984) *Nature 310*, 376−381.
4. Vis, H., Mariani, M., Vorgias, C. E., Wilson, K. S., Kaptein, R., and Boelens, R. (1995) *J. Mol. Biol. 254*, 692−703.
5. White, S. W., Appelt, K., Wilson, K. S., and Tanaka, I. (1989) *Proteins 5*, 281−288.
6. White, S. W., Wilson, K. S., Appelt, K., and Tanaka, I. (1999) *Acta Crystallogr. D 55*, 801−809.
7. Rice, P. A., Yang, S.-w., Mizuuchi, K., and Nash, H. A. (1996) *Cell 87*, 1295−1306.
8. Rice, P. A. (1997) *Curr. Opin. Struct. Biol. 7*, 86−93.
9. Broyles, S. S., and Pettijohn, D. E. (1986) *J. Mol. Biol. 187*, 47−60.
10. Hodges-Garcia, Y., Hagerman, P. J., and Pettijohn, D. E. (1989) *J. Biol. Chem. 264*, 14621−14623.
11. Paull, T., Haykinson, M., and Johnson, R. (1993) *Genes Dev. 7*, 1521−1534.
12. Bonnefoy, E., and Rouviere-Yaniv, J. (1991) *EMBO J. 10*, 687−696.
13. Lavoie, B. D., and Chaconas, G. (1993) *Genes Dev. 7*, 2510−2519.
14. Lavoie, B. D., Shaw, G. S., Millner, A., and Chaconas, G. (1996) *Cell 85*, 761−771.
15. Pontiggia, A., Negri, A., Beltrame, M., and Bianchi, M. E. (1993) *Mol. Microbiol. 7*, 343−350.
16. Bonnefoy, E., Takahashi, M., and Rouviere-Yaniv, J. (1994) *J. Mol. Biol. 242*, 116−129.
17. Castaing, B., Zelwer, C., Laval, J., and Boiteux, S. (1995) *J. Biol. Chem. 270*, 10291−10296.
18. Kamashev, D., Balandina, A., and Rouviere-Yaniv, J. (1999) *EMBO J. 18*, 5434−5444.
19. Kobryn, K., Lavoie, B. D., and Chaconas, G. (1999) *J. Mol. Biol. 289*, 777−784.

20. Segall, A. M., Goodman, S. D., and Nash, H. A. (1994) *EMBO J. 13*, 4536−4548.
21. Heyduk, T., and Lee, J. C. (1990) *Proc. Natl. Acad. Sci. U.S.A. 87*, 1744−1748.
22. Heyduk, T., Ma, Y., Tang, H., and Ebright, R. H. (1996) *Methods Enzymol. 274*, 492−503.
23. Hill, J. J., and Royer, C. A. (1997) *Methods Enzymol. 278*, 390−416.
24. Laue, T. M., and Stafford, W. F. (1999) *Annu. Rev. Biophys. Biomol. Struct. 28*, 75−100.
25. Cole, J. L., and Hansen, J. C. (2000) *J. Biomol. Techniques 10*, 163−176.
26. Fried, M. G., and Liu, G. (1994) *Nucleic Acids Res. 22*, 5054−5059.
27. Pinson, V., Takahashi, M., and Rouviere-Yaniv, J. (1999) *J. Mol. Biol. 287*, 485−497.
28. Sambrook, J., Fritsch, E. F., and Maniatis, T. (1989) *Molecular Cloning: A Laboratory Manual*, Vol. 2, 2nd ed., Cold Spring Harbor Laboratory Press, Cold Spring Harbor, NY.
29. Alberts, B., and Herrick, G. (1971) *Methods Enzymol. 21*, 198−217.
30. Hawkins, M. E., Pfleiderer, W., Mazumder, A., Pommier, Y. G., and Balis, F. M. (1995) *Nucleic Acids Res. 23*, 2872−2880.
31. Richards, E. G. (1975) in *Handbook of Biochemistry and Molecular Biology* (Fasman, G. D., Ed.) p 589, CRC, Cleveland, OH.
32. Lakowicz, J. R. (1983) *Principles of Fluorescence Spectroscopy*, Plenum Press, New York.
33. McGhee, J. D., and von Hippel, P. H. (1974) *J. Mol. Biol. 86*, 469−489.
34. Kowalczykowski, S. C., Paul, L. S., Lonberg, N., Newport, J. W., McSwiggen, J. A., and von Hippel, P. H. (1986) *Biochemistry 25*, 1226−1240.
35. Eftink, M. R. (1997) *Methods Enzymol. 278*, 221−258.
36. Hawkins, M. E., Pfleiderer, W., Balis, F. M., Porter, D., and Knutson, J. R. (1997) *Anal. Biochem. 244*, 86−95.
37. Jameson, D. M., and Sawyer, W. H. (1995) *Methods Enzymol. 246*, 283−300.
38. Fried, M., and Crothers, D. M. (1981) *Nucleic Acids Res. 9*, 6505−6525.
39. Grove, A., Galeone, A., Mayol, L., and Geiduschek, E. P. (1996) *J. Mol. Biol. 260*, 120−125.
40. Coombs, R. O., and Cann, J. R. (1996) *Electrophoresis 17*, 12−19.
41. Aki, T., and Adhya, S. (1997) *EMBO J. 16*, 3666−3674.
42. Lorenz, M., Hillisch, A., Payet, D., Buttinelli, M., Travers, A., and Diekmann, S. (1999) *Biochemistry 38*, 12150−12158.

BI002382R